First atmospheric compensation with a linearised high order adaptive mirror – ELECTRA

A. Zadrozny, M.P.J.L. Chang, D.F. Buscher, R.M. Myers,
A.P. Doel, C.N. Dunlop & R.M. Sharples

Physics Department, University of Durham,
South Road, Durham DH1 3LE, UK.

R.L. Arnold

ThermoTrex Corporation,
9550 Distribution Avenue, San Diego, CA 92121, USA.

ABSTRACT

Durham's ELECTRA AO system uses a 76 segment, 228 degree-of-freedom segmented mirror built by the ThermoTrex Corporation.

A novel feature of the mirror is the use of strain gauges to measure the displacements of the mirror's piezoelectric actuators. The strain gauge position measurements are used in a feedback control loop to linearise the response of the actuators. By removing piezo hysteresis as a source of positional error, the segments' piston displacement errors are reduced from 15% to $< 0.2\%$, improving the cophased tracking performance.

The strain gauge system has been used successfully with ELECTRA to demonstrate cophased near-IR operation on the 4.2m William Herschel Telescope, and we present measurements of its on-telescope performance.

1. INTRODUCTION

ELECTRA (76 **ELE**ment **C**ophasing and **TRA**cking) is Durham's second generation AO instrument, building on the experience gained with MARTINI[3,4] . It is a high order natural guide star system, intended to operate at visible and near-IR wavelengths. It will serve as a test-bed for developing novel AO techniques,[1] and will contribute elements of its hardware and control software to N*AO*MI,[7] the UK common-user infrared AO system for the William Herschel Telescope.

The instrument operates at the GHRIL Nasmyth platform of the 4.2 m William Herschel Telescope, La Palma. Its main elements are a 228 degree-of-freedom Segmented Mirror coupled to a 10×10 subaperture Shack-Hartmann wavefront sensor.

The WHT facility infrared camera, WHIRCAM, and facility optical CCDs are available as back-end instruments for ELECTRA, but two further instruments are being built at Durham to exploit the potential of ELECTRA for spectroscopy and interferometry. The first, TEIFU,[5] is a thousand fibre, high spatial resolution Integral Field Unit for the WYFFOS fibre spectrograph on the WHT. The second, DAFI,[2] is a fibre-fed dilute aperture interferometer. It serves as a test bed for single telescope mono-mode fibre interferometry.

The first part of this paper presents a general overview of ELECTRA, the second part is a more detailed account of the recently commissioned strain gauge linearisation system for the segmented mirror, and we conclude with a status report on the instrument.

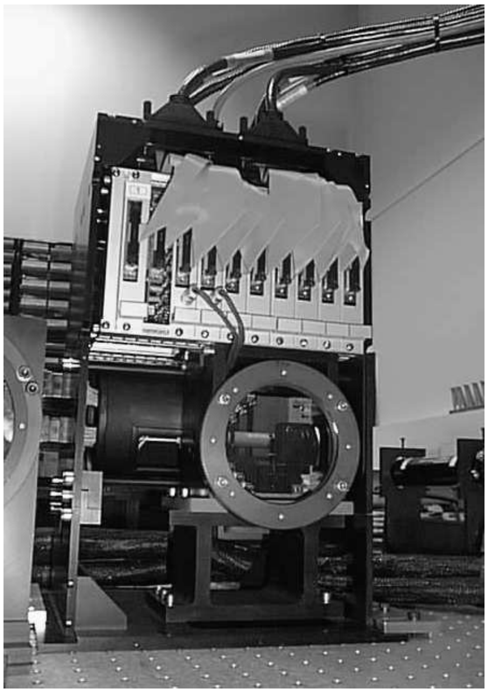

Figure 1. The Segmented Mirror, with the strain gauge amplifiers mounted above it. (The protective glass cover on the mirror is removed during operation.)

2. AN OVERVIEW OF ELECTRA

2.1. The Linearised Segmented Mirror

A principal feature of ELECTRA is the use of a high order segmented mirror (SM) as the wavefront correcting element. A segmented mirror has several attractive characteristics for astronomical adaptive optics.

The corrected wavefront needn't be continuous, and correction methods optimising parameters other than on-axis Strehl ratio can be adopted. For example, uncophased tip-tilt compensation by the individual segments offers modest image sharpening across a very large field of view. The scientific utility of this approach has been shown by the MARTINI instrument[8,9] .

Beyond its scientific versatility, an SM also offers certain technical advantages. When operated with a Shack-Hartmann WFS, a segmented mirror makes more efficient use of WFS light than a stacked actuator continuous facesheet mirror:

For wavefront aberrations produced through Kolmogorov turbulence, the wavefront fitting error per *segment* for a segmented mirror is $\sigma^2_{fit} \approx 0.18(s/r_0)^{5/3}$, ($s$ is the segment spacing, σ^2_{fit} is the variance in rad^2), whereas the fitting error per *actuator* for a stacked actuator continuous facesheet mirror is $\sigma^2_{fit} \approx 0.34(a/r_0)^{5/3}$, where a is the actuator spacing. There are three actuators per segment on a segmented mirror, so the fitting error per actuator is comparable for the two arrangements. However, when used with a Shack-Hartmann wavefront sensor, a segmented mirror has one Shack-Hartmann subaperture per segment, whereas a continuous facesheet mirror has one subaperture per actuator. That is, the fitting error per Shack-Hartmann subaperture, *and hence per incoming photon*, is lower for a segmented mirror. The more efficient use of guide star light is a significant potential advantage of segmented mirrors.

Also, a segmented mirror has a diagonal response matrix for single actuator tilts. That is, there are no interactions between subapertures inherent to the mirror itself, so computation of control signals need take no account of mirror modes.

Send correspondence to A.Z. E-mail: `Andrew.Zadrozny@durham.ac.uk`

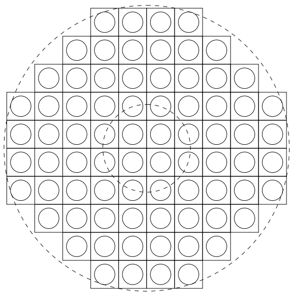

Figure 2. The layout of the segmented mirror, and its projection onto the primary mirror of the 4.2m William Herschel Telescope. Each segment projects onto a 42cm square at the primary mirror.

While the use of one Shack-Hartmann subaperture per segment has a fundamental sensitivity advantage, a general problem with this arrangement is that the segment has three degrees of freedom, tip, tilt and piston, but the Shack-Hartmann wavefront sensor measures only two of these, tip and tilt. Piston must be determined by numerical reconstruction of the wavefront, and can only be controlled in open loop. This relies on having a linear actuator response, but the piezo-electric materials used for segmented mirror actuators exhibit high hysteresis and non-linearity. Producing a linearised piston response is crucial to achieving good wavefront compensation performance with this kind of configuration.

One potential solution is to perform piston measurements *optically* in closed loop, with a fast figure-sensing interferometer. This provides a direct optical measurement of piston, but may require extremely high data rates if the interferograms are measured with a fast CCD camera. The issue of laser light contamination may also need to be addressed.

We have chosen to use strain gauges to linearise the actuator motion. The strain gauge displacement sensor is a mature sensor technology with well understood properties. When used in a digital closed loop to linearise our actuators, the data rates are in line with the other parts of the Real Time Control system. This approach provides a practical engineering solution to our linearisation requirement.

The segmented mirror (Figure 1) was built for us by ThermoTrex Corp. See Hulburd et al.[6] for a general account of the segmented mirror work at ThermoTrex. There are 76 segments arranged on a square grid (Figure 2). The segment spacing is 7.62mm, the individual mirrors are 7.54mm square, producing a 98% fill factor. The 0.08mm gaps between segments add 2% to the emissivity, a small increment given the number of warm optical surfaces in the beam. The mirror segments are aluminium-coated optical grade silicon, flat to 10 nm rms. Each segment can be driven in tip, tilt and piston, giving 228 degrees of freedom for the mirror as a whole.

The nominal end-to-end throw of the actuators is 6μm. The mirror is manufactured to have segments coplanar to 2μm. That is, 2μm of throw is used up to flatten the mirror, leaving 4μm of effective throw for atmospheric compensation.

2.2. The Optical Design

The optical design, shown in Figure 3, is based on a pair of on-axis paraboloids placed symmetrically around the Segmented Mirror. The first paraboloid collimates the incoming $f/11$ beam onto the SM, the second refocusses the beam onto the Wavefront Sensor and science arm. This simple configuration provides diffraction limited image quality across the $70''$ diameter field of view of the instrument. An IR-reflecting dichroic separates the WFS and science optical paths. A BaF_2/LiF doublet lens in the science arm forms the $f/55$ beam required by the WHIRCAM infrared camera. The CaF_2 field lens is there to form a pupil image on the WHIRCAM cold stop.

A very useful ancillary feature of the design is the inclusion of a Twyman-Green interferometer to measure the segmented mirror's optical figure. The interferometer lies clear of the main optical beam, allowing the mirror figure to be monitored at the same time as any other operation being performed with the instrument.

The wavefront sensor is a Shack-Hartmann type, with a 10×10 square array of microlenses aligned onto mirror segments. The WFS detector is an EEV CCD39 80×80 pixel four-port frame transfer CCD. Each Shack-Hartmann subaperture projects onto an 8×8 pixel subarray of the CCD. A choice of two alternative microlens

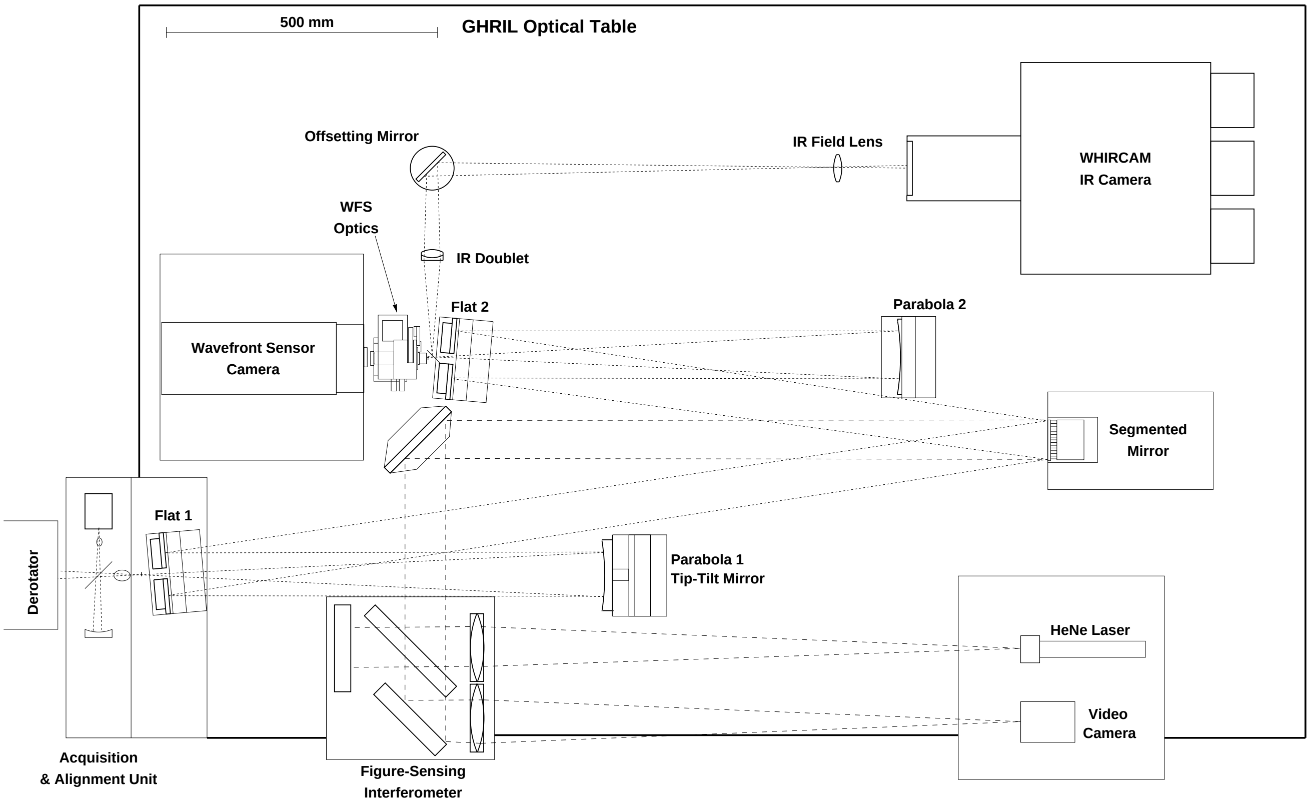

Figure 3. The ELECTRA optical layout, showing the configuration used at the WHT in July 1998. The optical path of the Figure-Sensing Interferometer is shown as the broader dashed line.

arrays is available, providing plates scales of 0.36″ per pixel (2.88″ per subaperture) and 0.27″ per pixel (2.16″ per subaperture). The latter scale provides better centroiding precision, the former gives more robust tracking performance in poor seeing.

The CCD readout camera was developed by the Central Laboratory of the Research Councils. This camera currently gives $12e^-$ read noise, with a maximum full frame rate of 1 kHz. Some additional work is being carried out to reduce read noise and implement on-chip pixel binning.

2.3. The Control System

The AO control loop processing is performed by a number of 320C44 digital signal processors in a VMEbus control computer. A multi-processor solution was required given the general level of CPU performance available when the development of ELECTRA began, and the CPU choice was strongly influenced by the need for a straightforward multi-processor implementation. The 320C44 DSPs each have a number of parallel data interface ports, called "comm-ports", which enable easy interconnection of several processors. For the ELECTRA controls implementation, all real-time data transfer between DSPs is over these comm-port connections, and all real-time data I/O is also over commport interfaces (Figure 4). The commport interface to the strain gauge analogue-to-digital converters is part of a commercial product, the interfaces to the WFS camera and segmented mirror drive were developed in-house.

Sixteen DSPs are connected together as two rings of eight processors. The Wavefront Sensor DSP Ring interfaces to the WFS camera, and performs Shack-Hartmann spot centroiding and wavefront reconstruction. Computation and data transfers on this ring are synchronised to the WFS CCD frame rate, typically between 167 Hz and 550 Hz. Each port of the four-port WFS CCD feeds data to one DSP, which computes Shack-Hartmann spot centroids for that quarter of the CCD. The centroid data are distributed over the Ring for

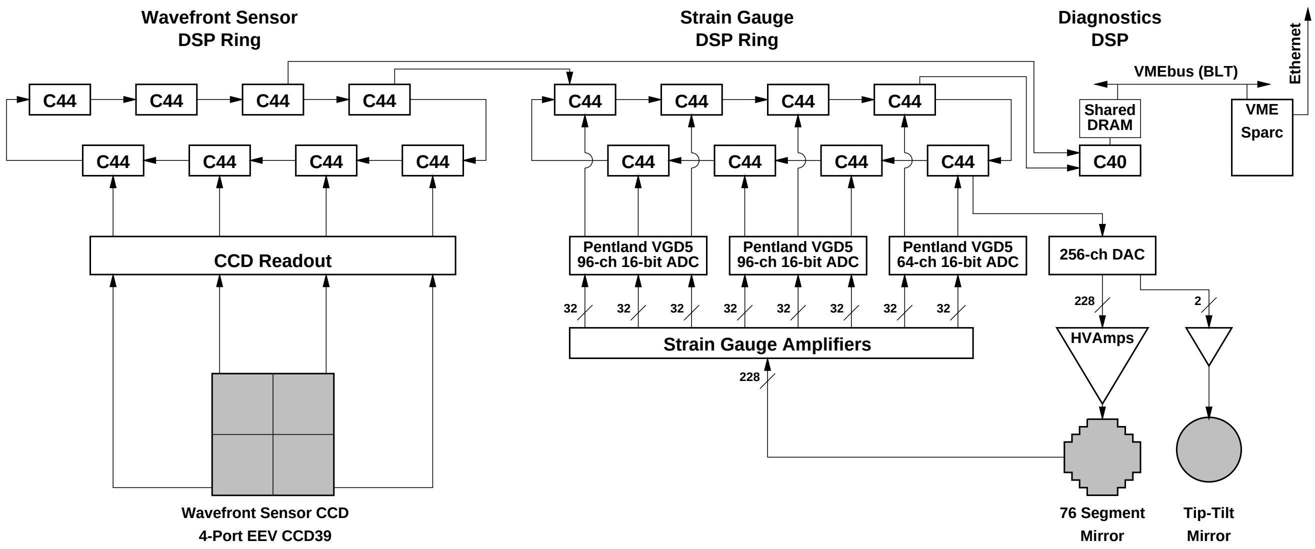

Figure 4. The ELECTRA Real Time DSP Control Architecture. The arrowed lines linking the 320C44 processors represent 'C40 comm-port connections. The lines below the CCD Readout and ADC stages represent analogue signal paths. The eight 320C44 DSPs on the Wavefront Sensor DSP Ring are mounted on a single LSI DBV44 VME carrier board. The eight DSPs on the Strain Gauge DSP Ring are on a second, identical board. The Diagnostics DSP is a single 320C40 processor on an LSI DBV46 VME board.

wavefront reconstruction, and the final mirror demand data are transmitted over a single commport connection linking the Wavefront Sensor DSP Ring to the Strain Gauge DSP Ring.

The Strain Gauge DSP Ring controls the strain gauge position feedback loop. It interfaces to the strain gauge analogue-to-digital converters, and to the digital-to-analogue converters feeding the segmented mirror's high voltage amplifiers. The Strain Gauge Ring is synchronised to the ADC sample rate, currently 1 kHz – 3.3 kHz, and receives mirror demand data asynchronously from the Wavefront Sensor DSP Ring. The strain gauge data acquisition system is described in more detail in a later section.

The Diagnostics DSP receives diagnostic data, such as WFS centroids and mirror demand arrays, from both DSP rings. Its purpose is to provide a fast data path between the real-time DSPs and general purpose workstations elsewhere in the system. The DSP doesn't process the data, it simply buffers the data stream in local memory and transfers it over a fast (block transfer) VME interface to an embedded Sparc processor in the VME crate. The data are processed on this Sparc, or sent on to a visualisation computer networked to it. The decision to adopt a fast data link to a Unix workstation, in preference to performing diagnostics processing on the DSPs themselves, was taken to enable flexible and convenient programming of diagnostic functions on a made-to-order basis.

The Segmented Mirror actuators are driven by $\pm$210 V high voltage amplifiers, developed at Durham and based on the Apex PA87 part. The drive frequency is limited to $<$1 kHz, to avoid the 2.4 kHz mechanical resonance of the PZT actuators.

As well as the main AO control system, there is also a simple EPICS based mechanisms computer controlling several motorised translation stages and miscellaneous mechanisms on the optical bench.

3. STRAIN GAUGE LINEARISATION OF THE SEGMENTED MIRROR

3.1. The Actuator Design

Each mirror segment is a tube of PZT–5H ceramic with an optical grade silicon mirror attached at one end. The monolithic tube provides three degrees of freedom; three electrodes, running down the length of the tube 120° apart, are deposited on the outer surface, and a common ground electrode covers the inner surface. A voltage applied across the wall of the tube deforms the ceramic in the perpendicular direction, increasing or decreasing the length of the tube at one electrode. Position sensing strain gauges are attached within the segment as shown

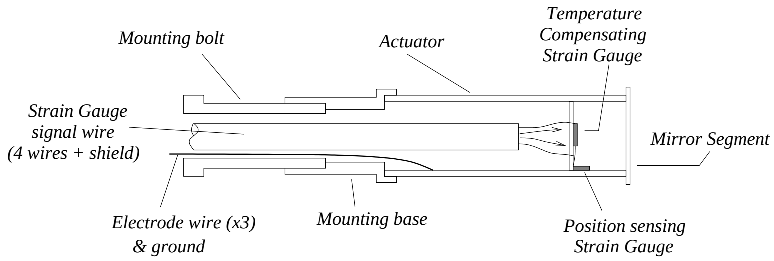

Figure 5. The cross-section of a segment, showing the strain gauge locations. Three position-sensing strain gauges are attached around the inner wall of the ceramic tube, and three matched temperature compensating strain gauges are attached to an alumina ceramic disk fitted within the tube. *(Length not to scale.)*

Actuator Parameters	
Actuator Material	Lead Zirconate Titanate (PZT) Ceramic
Actuator Dimensions	27.0 mm Length, 5.84 mm Outer Diameter
End-to-End Throw	6 μm, at $\pm$ 215 V Applied Voltage
Actuator Capacitance	6 nF $\pm 5\%$
Resonance Frequency	2.4 kHz
Strain Gauge Parameters	
Strain Gauge Model	Entran ESU–025–500
Strain Gauge Material	P–Type Silicon
Strain Gauge Active Length	0.625 mm
Nominal Resistance	500 Ω $\pm 10\%$
Gauge Factor $\frac{\Delta R/R}{\Delta L/L}$	$+140$ $\pm 5\%$

Table 1. The physical and electrical parameters of the linearised actuator.

in Figure 5. Temperature compensating strain gauges are fitted to a ceramic disk in the PZT tube. The main parameters of the actuator are summarised in Table 1.

3.2. The Strain Gauge Data Acquisition System

The strain gauge system is intended for common-user operation with N*AO*MI, as well as its current use with ELECTRA. This influenced several design choices during its implementation:

The strain gauge bridge offset varies from actuator to actuator, as do the SG response and loop gain, due to variations in strain gauge mounting. For a >200 channel system, periodic manual adjustment of these parameters (e.g. by trimpots) would be tedious at best, and unacceptable for common-user operation. Automated adjustment of some sort is required, either by computer controlled adjustments to an analogue feedback circuit, or by full digital control. Software access to the strain gauge signal itself is needed for diagnostic purposes, and it was also considered desirable to allow for future modification and enhancement of the strain gauge control law in software, rather than to hard-wire the feedback circuit. For these reasons, a digital control loop implementation was chosen in preference to an analogue one.

The strain gauge amplifier rack is mounted immediately above the segmented mirror (Figure 1). A very compact top-mounted configuration was needed to meet N*AO*MI space constraints, and power dissipation on the optical bench had to be kept low. (The amplifier rack dissipates 4 W in total.) A simple circuit at the mirror end was called for:

Each pair of position-sensing and temperature-compensating strain gauges is wired in a balanced bridge configuration to an instrumentation amplifier (Figure 6). The balancing resistors aren't adjustable – the residual offset is removed numerically after A-D sampling. While this somewhat degrades common-mode rejection and requires higher ADC resolution, it combines a compact circuit with fully automatic operation. The amplified signal is fed from the optical bench to the control computer in the next room.

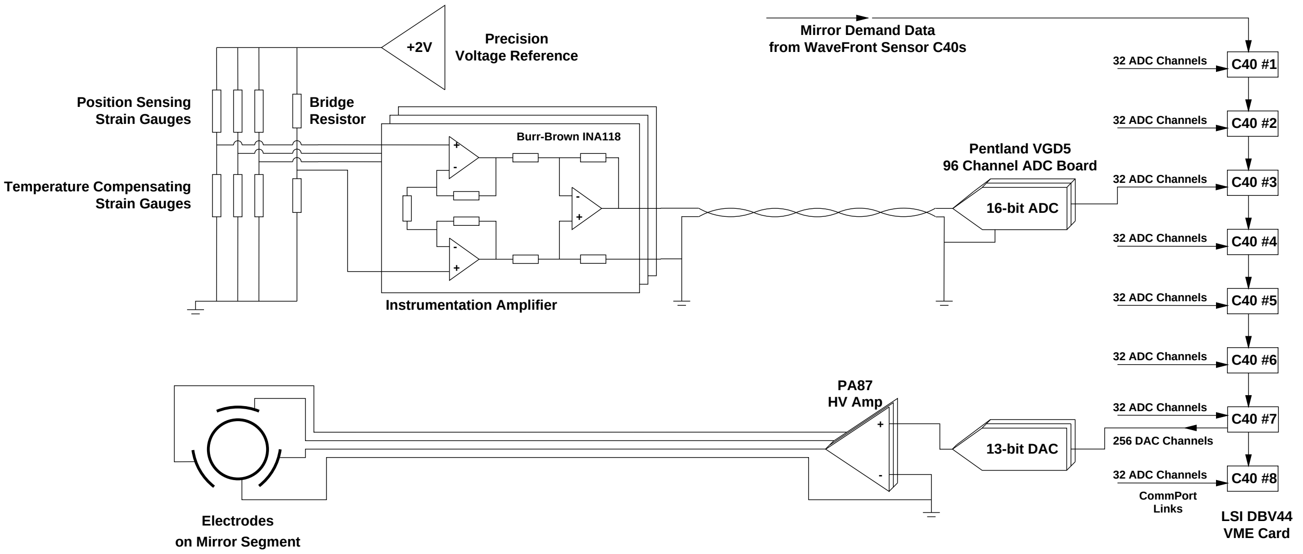

Figure 6. The analogue signal interface to the strain gauges and the actuator electrodes of a single mirror segment, and the data interface to the strain gauge DSP control system.

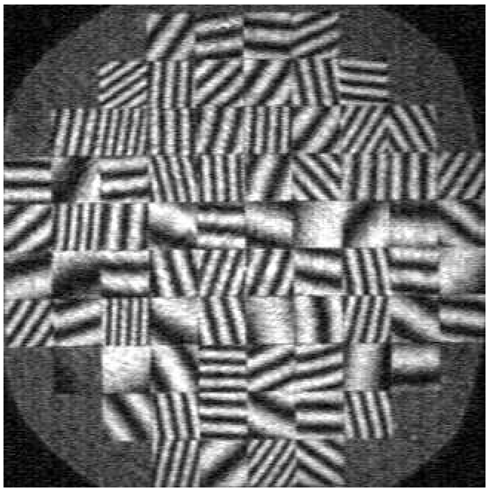

Figure 7. The Segmented Mirror viewed by the Figure-Sensing Interferometer ($\lambda = 633$ nm).

Analogue-to-digital conversion is performed by Pentland VGD5 ADC boards. These commercial VME cards provide 96-channels of 16-bit conversion at an 85 kHz all-channel maximum sampling rate. They also provide LSI Commport connections as one of their optional data interfaces, giving a direct connection into our I/O scheme. The combination of sampling performance and versatile data interfacing made these an ideal choice for our purpose. The nominal ADC resolution is 1 ADU = 6.1 nm of Optical Path Difference on the Segmented Mirror, where the OPD is twice the mirror movement.

Each group of 30 ADC channels (one mirror column) is connected by a commport link to one 320C44 processor on an LSI DBV44 VME carrier board. The software control law on the feedback loop is currently a simple integrator. The strain gauge sample rate is presently limited to 3.3 kHz by the CPU load. We hope to achieve a $\sim$10 kHz rate soon, by modifying and optimising the control software.

3.3. Evaluation of Strain Gauge Performance

The linearity of the strain gauges is the key to their performance. Measurements of linearity were made using the standard ELECTRA optical set-up. The actuator displacement was measured interferometrically with the

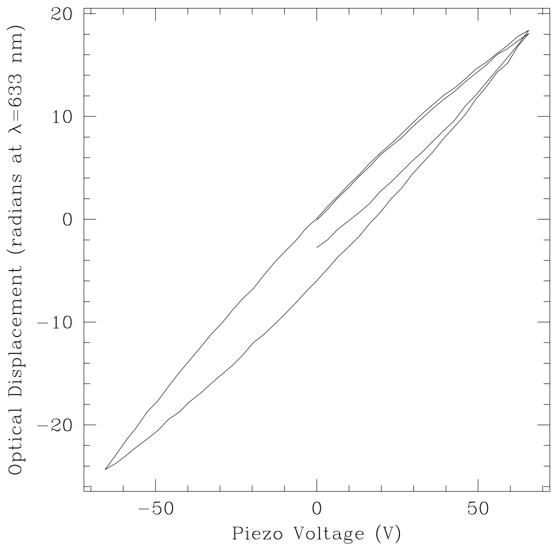

Figure 8. The hysteresis loop of one actuator, over about one third of its range, measured interferometrically. The actuator exhibits 15% hysteresis.

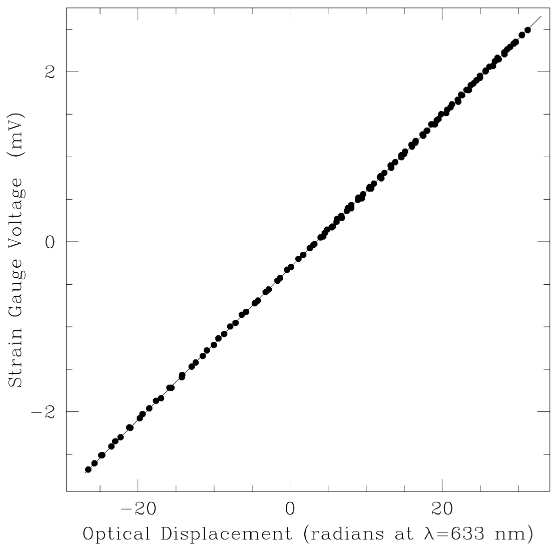

Figure 9. Interferometric measurement of strain gauge linearity. The strain gauges are linear to better than $\lambda/157$ at λ=633 nm.

Twyman-Green figure-sensing interferometer present on the instrument. The interferometer's light source is a HeNe laser ($\lambda = 633$ nm), the detector is a video camera connected to a computer frame grabber. Figure 7 shows an image of a typical interferogram recorded by this system. Segment displacements were determined from Fourier analysis of the fringe movement, and compared to strain gauge readings.

Air turbulence along the interferometer path introduced significant fringe motion. Two mirror segments adjacent to the segment of interest were held stationary, and measurements of their phases were made to compensate for these fluctuations.

Figure 8 illustrates why the strain gauges are needed; it shows the uncorrected hysteresis loop of an actuator, scanned across a third of its range, measured by the interferometric set-up described above. There is just under 15% hysteresis, corresponding to 1.8μm of optical path difference for an end-to-end motion. While typical piston excursions in closed loop will be smaller that the maximum throw, it's clear that these errors would rule out cophased operation at visible wavelengths.

Figure 9 shows strain gauge readings against the true optical position over roughly the same interval. The scatter is due to errors in the interferometric phase measurement. The maximum deviation from the best fit straight line is $< \lambda/157$ at $\lambda = 633$ nm.

Noise measurements in the telescope environment were made during the July 1998 WHT commissioning run. The typical measurement noise at the telescope was 2 ADU, or 12 nm rms of optical path. This is $\lambda/40$ at $\lambda = 500$ nm, contributing 2% of Strehl degradation to the error budget at $\lambda = 500$ nm, and 0.1% at $\lambda = 2.2$ μm.

The total displacement error due to non-linearity and noise is <0.2% of the end-to-end throw. This introduces a negligible performance degradation at infrared wavelengths, and the degradation in the visible is small.

Thermal drift of the strain gauge signal also has to be dealt with. The variation of strain gauge resistance with temperature is approximately cancelled out by the use of matched temperature compensating strain gauges in the actuators. However, a residual variation with temperature remains, and there are higher order temperature effects not removed by this circuit. Notably, the gauge factor $\frac{\Delta R/R}{\Delta L/L}$ (R is strain gauge resistance, L is strain gauge length) varies with temperature. Temperature sensors are built into the Segmented Mirror mount, and work is currently underway to calibrate the remaining thermal variations.

4. ELECTRA OPERATION AND STATUS

4.1. Alignment of the Segmented Mirror

A key optical alignment issue for the instrument is the initial co-phasing of mirror segments to produce a flat optical surface on the Segmented Mirror. ELECTRA's Twyman-Green interferometer can't cophase the mirror segments. It operates with a monochromatic light source because the interferometer arms are of unequal length, therefore it can be used to flatten the mirror only to modulo-λ. Instead, mirror flattening is carried out by adapting the Shack-Hartmann wavefront sensor to operate as an interferometer: The microlens array is first offset by half a subaperture along one axis. When illuminated by a white light alignment source, this combines light from every pair of adjacent mirror segments to produce an array of interference fringes, instead of Shack-Hartmann spots, on the WFS detector. The position of the central fringe within each subaperture is a measure of the relative piston displacement between those two segments, so measurements of the fringe positions are used for pair-wise alignment of the segments, one axis at a time.

4.2. Project Status

ELECTRA's first commissioning run took place on the William Herschel Telescope in June 1997, when its initial mode of operation, un-cophased tip-tilt correction of the individual segments, was demonstrated. Its second observing run, in July 1998, added the strain gauge linearisation system and fully cophased operation for near-IR observations. Figure 10 illustrates the level of correction that was achieved. Closed loop compensation worked well, and a diffraction-limited image core was regularly achieved, but the image quality was degraded by a high level of non-common path astigmatism. This fixed aberration exceeded the offset range of a WFS subaperture, and couldn't be corrected in closed loop. The source of the aberration in the science path is being investigated.

While system performance was limited by the uncorrected non-common path aberration, we were encouraged that the strain gauge linearisation of the Segmented Mirror proved very effective, and excellent cophased tracking in the H and K bands was obtained.

Some final commissioning effort, and a first round of science observations, is expected in the first half of 1999. The TEIFU integral field unit will follow soon after, and the ELECTRA segmented mirror, with its associated strain gauge and high voltage drive electronics and real-time control system, will begin operating with the N*AO*MI common-user infrared AO system on the William Herschel Telescope.

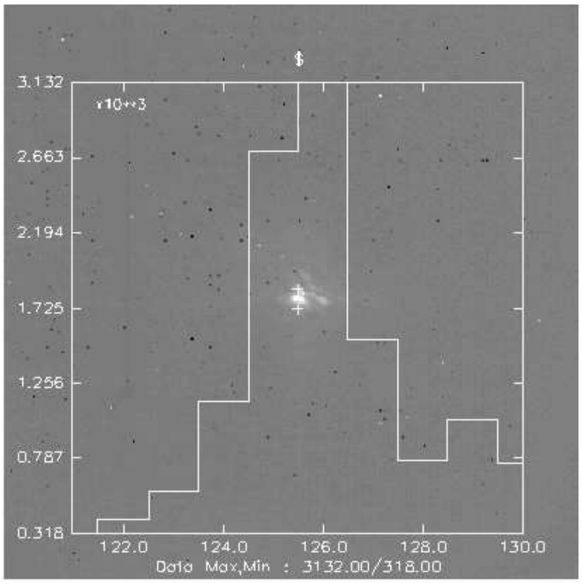

Figure 10. An AO corrected long exposure image of N21+37, taken with the WHIRCAM infrared camera at $\lambda = 2.1\mu$m. The exposure time is 15s, the plate scale is $0.05''$ per pixel. The extended structure in the PSF is caused by non-common path astigmatism in the infrared (science) arm.

5. ACKNOWLEDGEMENTS

ELECTRA is funded by PPARC. The Wavefront Sensor Camera was funded by a grant from the Royal Society Paul Instrument Fund. The William Herschel Telescope is operated on the island of La Palma by the Isaac Newton Group in the Spanish Observatorio del Roque de los Muchachos of the Instituto de Astrofísica de Canarias.

REFERENCES

1. Buscher D.F., Doel A.P., Andrews N., Dunlop C., Morris P.W., Myers R.M., Sharples R.M., Vick A., Zadrozny A., Haniff C.A., Wilson R.W., 1995, in *Topical Meeting on Adaptive Optics*, ESO Conf. and Workshop Proc. No. **54**, ed. M. Cullum, p.63
2. Chang M.P.J.L., Buscher D.F., 1998, Proc. SPIE **3350**, p.2
3. Doel A.P., Dunlop C.N., Major J.V., Myers R.M., Sharples R.M., 1991, Proc. SPIE **1542**, p.319
4. Doel P., Buscher D., Dunlop C., Sharples R., Andrews N., 1995, in *Topical Meeting on Adaptive Optics*, ESO Conf. and Workshop Proc. No. **54**, ed. M. Cullum, p.69
5. Haynes R., Doel A.P., Content R., Allington-Smith J., Lee D., 1998, Proc. SPIE **3355**, p.788
6. Hulburd W.G., Barrett T.K., Cuellar L., Sandler D.G., 1992, Proc. SPIE **1543**, p.64
7. Longmore A., Wells M., Strachan M., Dixon C., Peacocke T., Myers R., Humphreys R., Gentles B., Worswick S., Weise A., 1997, Proc. SPIE **3126**, p.18
8. Shanks T., Tanvir N.R., Major J.V., Doel A.P., Dunlop C.N., Myers R.M., 1992, MNRAS **256**, 29p
9. Tanvir N.R., Shanks T., Major J.V., Doel A.P., Dunlop C.N., Myers R.M., Redfern R.M., O'Kane P., Devaney M.N., 1991, MNRAS **253**, 21p